

Flavor and path-length dependence of jet quenching from inclusive jet and γ -jet suppression

Agnieszka Ogrodnik, Martin Rybář, and Martin Spousta

Institute of Nuclear Physics, Faculty of Mathematics and Physics, Charles University

Received: date / Revised version: date

Abstract. We use the parametric approach to analyze jet suppression measured using the nuclear modification factor of inclusive jets, b -jets, and jets from γ -jet events. With minimum model assumptions, we quantify the magnitude of the average energy loss and its transverse momentum dependence. Then, we quantify the impact of fluctuations in the energy loss and nuclear PDFs on the measured jet suppression. Employing the Glauber model to infer the information about the collision geometry, we quantify the path-length dependence of the average energy loss, which is shown to be consistent with that expected for the radiative energy loss. Using the obtained parameterizations, we evaluate jet v_2 , obtaining results consistent with measurements. We also provide model-independent predictions for the magnitude of energy loss expected in upcoming oxygen-oxygen collisions. Finally, we analyze intriguing features seen in the suppression of jets in the γ -jet system.

PACS. XX.XX.XX No PACS code given

1 Introduction

Calculations of lattice quantum chromodynamics (QCD) predict the emergence of deconfined matter in ultra-relativistic collisions of heavy-ions [1]. This type of matter composed of quarks and gluons freed from hadrons, which is also called quark-gluon plasma (QGP), existed during the first microseconds of the evolution of the universe [2]. It is, therefore, of importance to study the properties of QGP and the mechanisms of its interaction with elementary particles passing through it. Such studies may be performed using jets of hadrons originating in a hard scattering of elementary quarks and gluons occurring within the volume of QGP medium. Jets are described in perturbative QCD as virtuality-ordered and/or angular-ordered showers of partons propagating through the vacuum. When passing the QGP medium, partons from the parton shower lose the energy predominantly by medium-induced radiative processes [3, 4, 5, 6]. This leads to modification of yields and structure of jets with respect to those passing only the vacuum [7, 8, 9]. This phenomenon is commonly termed jet quenching.

One of the important open questions related to jet quenching is how much the energy loss depends on the color charge of the initial parton [10, 8]. This color charge dependence may have two qualitatively different origins. First, it may originate as a consequence of the structure of the parton shower, which is, on average, different for quark-initiated and gluon-initiated jets [11, 12]. Quark-initiated jets, which typically produce harder and narrower parton showers with fewer constituents, may naturally be expected to lose less energy than gluon-initiated jets, which have softer and wider parton showers with more constituents. This principle is encoded in many theoretical descriptions in different ways, compare e.g. Refs. [13, 14, 15], and it is also implemented in jet quenching Monte-Carlo generators [16, 17, 18, 19, 20, 21]. Second, the color charge dependence of the energy loss may be connected with the phenomena of color (de)coherence [22, 23]. In that picture, a substantial part of the parton shower loses the energy coherently. The energy loss is then driven by a color charge of the initial quark or gluon. Besides analytical calculations of color coherent energy loss [22, 24, 25, 23, 26, 27, 28], the color coherence starts to be discussed in the context of Monte-Carlo (MC) simulations of jet quenching as well [29, 30, 31].

In addition to the incoherent and color-coherent regimes of in-medium emissions, an admixture of vacuum-like emissions [32] may also contribute to the overall observable jet quenching. To address the original question on the role of jet flavor in this complex physics setup, detailed studies comparing observables having different sensitivity to the flavor of the initial parton need to be performed. One example of such studies is the study suggesting measurements of

Correspondence to: martin.spousta@matfyz.cuni.cz

forward jet substructure [33], which, however, have not yet been measured in Pb+Pb collisions at the LHC. Another possibility to study the flavor sensitivity may come from measurements of jets originating in γ -jet final state [34], which offer a sample dominated by quark-initiated jets [35]. For this final state, multiple measurements were performed at the LHC [35, 36, 37, 38, 39, 40, 41, 42]. Understanding the jet production in the γ -jet final state provides not only a tool to study the flavor dependence, but it should also allow a better understanding of the role of selection biases and the path-length dependence of the energy loss [43, 44, 45]. Here, in particular, the quantitative assessment of path-length dependence of parton energy loss remains an open issue for a long time [46, 47, 48, 49]. Studying similarities and differences between the inclusive jet suppression and suppression of jets from γ -jet final state is therefore of a crucial importance.

In this paper, we apply the parametric approach to jet quenching (also dubbed ‘‘EQ-model’’) [50, 51] to benchmark the impact of different components contributing to the final observable jet quenching. The paper is organized as follows. Section 2 introduces and extends the parametric modeling of jet quenching. Section 3 discusses the simulation of input MC samples used in the study. Section 4 quantifies the magnitude of the jet quenching in inclusive jets and compares the ability of different parametric implementations to reproduce measured jet R_{AA} . Section 5 extracts the path-length dependence of jet suppression using Glauber modeling and reproduces the measured data on jet v_2 . The differences between the inclusive jet suppression and suppression of b -jets are also briefly discussed in that section. In Section 6, extracted parameters of jet quenching from inclusive jet R_{AA} are used to study the suppression of jets in the γ -jet system. The last section then provides a summary and conclusions.

2 Parametric approach to parton energy loss

In Ref. [50], the parametric approach to the jet quenching modeling was introduced. The basic ingredient of the modeling is the approximation in which observable jet spectra consist of two components: quark-initiated jet spectra and gluon-initiated jet spectra. Individual spectra are precisely parameterized using the modified power law, and combined spectra are then expressed as,

$$\frac{dN}{dp_T^{\text{jet}}} = A \sum_{i=1}^2 f_{i,0} \left(\frac{p_{T0}}{p_T^{\text{jet}}} \right)^{n_i(p_T^{\text{jet}})}, \quad (1)$$

where A is the normalization factor, p_{T0} is an arbitrary parameter to keep the exponent dimensionless (here, $p_{T0} = 40$ GeV is used). The index $i = 1, 2$ labels quark-initiated and gluon-initiated jets, respectively, and $f_{i,0}$ is a fraction of quark-initiated or gluon-initiated jets at p_{T0} ($f_{1,0} = 1 - f_{2,0}$). The exponent n_i is p_T^{jet} dependent,

$$n_i(p_T^{\text{jet}}) = \sum_{j=0}^{j_{\text{max}}} \beta_j \log^j \left(\frac{p_T^{\text{jet}}}{p_{T0}} \right). \quad (2)$$

Here β_j are free parameters, and $j_{\text{max}} = 2$ was reported to allow sufficient precision in the parameterization of jet spectra.

The average transverse momentum lost by the jet is then expressed as

$$\langle \Delta p_T^{\text{jet}} \rangle_i = c_{F,i} s \left(\frac{p_T^{\text{jet}}}{p_{T0}} \right)^\alpha, \quad (3)$$

where $i = 1, 2$ as in Eq. (1) and $c_{F,i}$, α , and s are free parameters. The color factor $c_{F,1}$ for quark-initiated jets is set to unity and $c_{F,2}$ for gluon-initiated jets is labeled c_F .

The quantification of energy loss using Eq. (3) then allows to derive the analytical expression for the jet nuclear modification factor,

$$R_{AA} = \frac{dN_Q}{dp_T^{\text{jet}}} \bigg/ \frac{dN}{dp_T^{\text{jet}}} = \sum_{i=1}^2 f_i(p_T^{\text{jet}}, n_i, f_{i,0}) g_i(p_T^{\text{jet}}, n_i, \langle \Delta p_T^{\text{jet}} \rangle_i) \quad (4)$$

where f_i is the flavor fraction given by

$$f_i = \left[1 + \frac{f_{2,0}}{f_{1,0}} \left(\frac{p_T^{\text{jet}}}{p_{T0}} \right)^{n_1(p_T^{\text{jet}}) - n_2(p_T^{\text{jet}})} \right]^{-1} \quad (5)$$

and g_i is an analytical function calculated in [50]. The analytical expression for the parameterized R_{AA} then allows conveniently fitting the data. Besides the analytical approach, MC simulation can also be performed by modifying the momentum of quark- and gluon-initiated jets delivered by the MC generator using Eq. (3). Modified spectra for the two flavors can then be combined and divided by original spectra with no modification in order to obtain the R_{AA} . The simulated R_{AA} can be compared with the data to obtain parameters minimizing the difference between the data and the simulated R_{AA} . Initial unmodified jet spectra can either be delivered directly by the MC generator or the output from the MC generator can be parameterized by Eq. (1) separately in rapidity intervals, and jets may be obtained by sampling from the parameterized spectra. This later approach is used in this study.

In the first study using the LHC run-1 data at $\sqrt{s_{NN}} = 2.76$ TeV [50], c_F was fixed to the leading order value of $9/4$, and $\alpha = 0.55$ was found to describe the data well. In the subsequent study which used rapidity dependent LHC run-1 data [51], following values of parameters were determined: $c_F = 1.78 \pm 0.12$, $\alpha = 0.52 \pm 0.02$, and s depending linearly on N_{part} .

Going beyond the approach of average energy loss, one may introduce fluctuations by convoluting the single jet spectrum with the energy loss distribution $w(p_T^{\text{jet}}, \Delta p_T^{\text{jet}})$

$$\frac{dN_Q}{dp_T^{\text{jet}}} = \int d\Delta p_T^{\text{jet}} \frac{dN}{dp_T^{\text{jet}}} w(p_T^{\text{jet}}, \Delta p_T^{\text{jet}}), \quad (6)$$

where Δp_T^{jet} is connected with the average energy loss by

$$\langle \Delta p_T^{\text{jet}} \rangle = \int d\Delta p_T^{\text{jet}} \Delta p_T^{\text{jet}} w(p_T^{\text{jet}}, \Delta p_T^{\text{jet}}). \quad (7)$$

One may further assume, as e.g. in Ref. [52], that w depends only on $p_T^{\text{jet}} / \langle \Delta p_T^{\text{jet}} \rangle \equiv x$. To model the energy loss distribution, a generalized integrand of gamma function can be used,

$$w(x) = \frac{c_1^{c_0}}{\Gamma(c_0)} x^{c_0-1} e^{-c_1 x}, \quad (8)$$

where c_0 and c_1 are free parameters. For $c_0 = c_1$, the functional form (8) coincides with functional form used in previous studies [53, 52, 54]. Setting $c_0 \neq c_1$ allows parameterizing fluctuations used in recent boson-jet study [55].

Besides introducing parameterization of fluctuations, one may further generalize the power-law functional form to allow logarithmic p_T^{jet} dependence,

$$\langle \Delta p_T^{\text{jet}} \rangle = c_F s \left(\frac{p_T^{\text{jet}}}{p_{T0}} \right)^\alpha \log \left(\frac{p_T^{\text{jet}}}{p_{T0}} \right). \quad (9)$$

This parameterization keeps the same number of free parameters as (3), and it is used, e.g., in studies performed with the linear Boltzmann transport (LBT) model [52].

3 Input parton spectra

The inclusive jet production used in this study is simulated using PYTHIA8 [56, 57] with A14 tune [58] and a NNPDF 2.3 LO PDF set [59] which was used as a reference in recent experimental studies of jet production in pp collisions at 5.02 TeV [60]. As an alternative, inclusive jets simulated using HERWIG7 [61] are used. The PYTHIA and HERWIG samples are often used together in order to provide a systematic check of the flavor dependence of jet production [62, 63], which is known to be simulated differently in these two Monte-Carlo (MC) generators. To reconstruct jets, the anti- k_t algorithm [64] implemented in FastJet package [65] is used with the default value of distance parameter $R = 0.4$ ($R = 0.2$ jets are used in a brief study of b -jets). The γ -jet production is simulated using PYTHIA8 with A14 tune and a NNPDF 2.3 LO PDF set. To match the conditions of analysis in Ref. [35], photons are required to be isolated, have $p_T^\gamma > 50$ GeV, and $|\eta| < 2.37$. Photons are isolated if the sum of transverse energy within the $R = 0.3$ cone around the photon is less than 3 GeV. Selected jets have $p_T^{\text{jet}} > 50$ GeV, $|\eta| < 2.8$ and are opposite to selected photons in the azimuthal angle ($\Delta\phi_{\gamma, \text{jet}} > 7\pi/8$). The γ -jet cross-section measured in pp collisions has two contributions, one from photons originating directly in the hard scattering ('prompt photons') and one from photons originating in the fragmentation of a jet in a dijet system ('fragmentation photons'). In the simulation by PYTHIA8, the later contribution constitutes 35% of the total cross-section for jets within the studied kinematic range and cannot, therefore, be neglected. As an alternative, γ -jet production is simulated also using HERWIG7 with MMHT2014lo [66] PDF set. Simulation is done separately for samples with fragmentation photons and prompt photons.

The magnitude of the difference between the shape of simulated jet spectra and jet spectra measured in 5.02 TeV pp collisions [67] is smaller than approximately 20% for both the inclusive jets and γ -tagged jets in both PYTHIA8

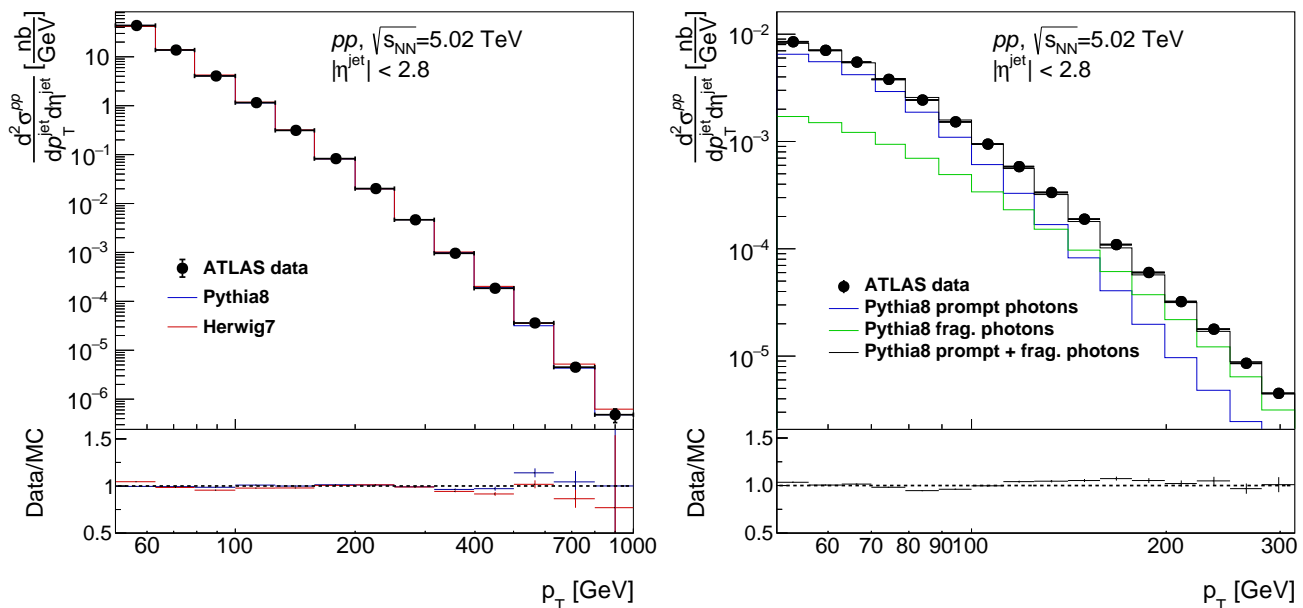


Fig. 1. *Left:* Cross-section for the inclusive jet production from PYTHIA8 and HERWIG7 compared with the data [67]. *Right:* Cross-section for the jet production in γ -jet system from PYTHIA8 along with individual contributions from prompt and fragmentation photons compared with the data [35]. A reweighting discussed in the text is applied on both MC cross-sections. The ratio of data to MC is shown in lower panels.

and HERWIG7. The jet p_T spectra for inclusive jet samples are reweighted before parameterization (Eq. (1)) to reduce this difference. The reweighting factors are obtained by fitting the data-to-MC ratio by a fifth-order and fourth-order polynomial in p_T^{jet} in the case of PYTHIA8 and HERWIG7, respectively. The same reweighting is applied on quark-initiated and gluon-initiated jets. In the case of γ -tagged jets, a two-step reweighting procedure is applied. First, the prompt photon and fragmentation photon contributions are scaled by constant weights such that the χ^2 defined using the difference between the pp data and MC is minimized. To further improve the data-to-MC ratio, a third-order polynomial in p_T^{jet} is used to reweight jet spectra connected with prompt photons. Alternatively, the reweighting is applied on jet spectra connected with fragmentation photons. In general, the differences in the resulting R_{AA} between reweighted and original spectra are rather small and are quantified later in the paper.

The comparison of the parameterization of the final reweighted MC spectra to the 5.02 TeV pp data is shown in Figure 1. The left panel of Figure 1 shows p_T^{jet} spectra for inclusive jets, and the right panel shows spectra for jets from γ -jet events. One may see that parameterizations of jet p_T spectra are consistent with the data within statistical uncertainties. These parameterizations are used to evaluate the denominator of R_{AA} .

To simulate the initial state effects in lead-lead collisions, additional samples for both the inclusive jet production and γ -jet production in PYTHIA8 are produced using correction for the isospin effect and EPPS16 NLO nuclear parton distribution functions (nPDF) [68]. Jet spectra with nPDF and isospin effects are reweighted by factors discussed above, and they are then parameterized using Eq. (1). Unless stated otherwise, these parameterizations are used in the numerator of R_{AA} .

4 Suppression of inclusive jets

To determine the free parameters for various jet quenching parameterizations discussed in Sec. 2, the inclusive jet R_{AA} measured by ATLAS is used [67]. The parameters are extracted by a multidimensional minimization procedure based on Minuit [69] similar to that used in [51]. The ability of a given parameterization to describe jet R_{AA} data is quantified in terms of χ^2/ndof evaluated as a difference between the model and the data for the R_{AA} measured differentially in p_T^{jet} and centrality.

First, it is found that jet R_{AA} from [67] measured inclusively in rapidity is unable to constrain c_F . As a default value of c_F we therefore use $c_F = 1.78$, which was found in the previous study using Run-1 data measured differentially in rapidity [51]. The value determined in that study ($c_F = 1.78 \pm 0.12$) is consistent with the value of effective color charge calculated and measured for the vacuum jets with hardness $Q \approx 100$ GeV [70, 71] and it is also consistent

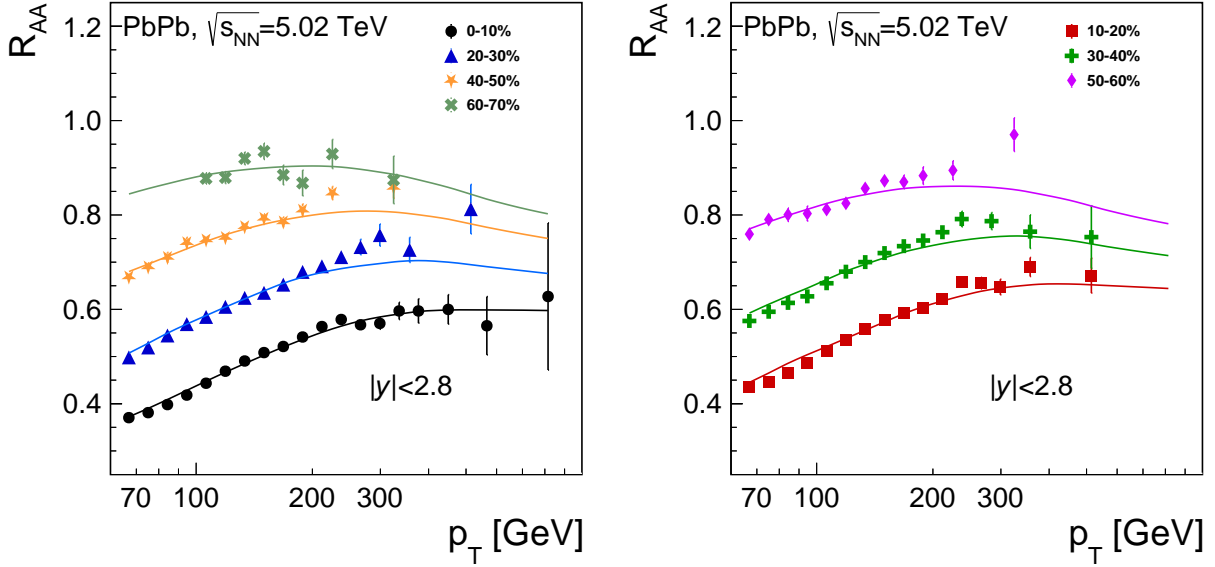


Fig. 2. Measured jet R_{AA} [67] (data points) compared to the parameterization p1 of jet quenching (solid line), which provides the best description of the data (for details on parameterization p1, see the text).

Label	Formulae	Spectra	Parameters	References	$\chi^2 _{0-10\%}$	$\chi^2 _{\text{all}}$
p1	(3),(8)	P8, nPDF	$\alpha_{\min} = 0.27, c_F = 1.78$	[51, 72]	0.51	1.06
p2	(3),(8)	P8, nPDF	$\alpha_{\min} = 0.24, c_F = (9/4)^{1/3}$	[51, 72, 18]	0.53	1.05
p3	(3),(8)	P8, nPDF	$\alpha_{\min} = 0.29, c_F = 9/4$	[51, 72]	0.50	1.09
p4	(3),(8)	P8	$\alpha_{\min} = 0.33, c_F = 1.78$	[51, 72]	0.70	1.06
p5	(3),(8)	H7	$\alpha_{\min} = 0.30, c_F = 1.78$	[51, 72]	0.88	1.18
p6	(3)	P8, nPDF	$\alpha_{\min} = 0.40, c_F = 1.78$	[51]	0.62	1.53
p7	(9),(8)	P8, nPDF	$\alpha_{\min} = 0.15, c_F = 1.78$	[53]	0.44	1.43

Table 1. Definitions of parameterizations of p_T^{jet} dependence of jet quenching along with parameter α obtained by minimization with respect to measured jet R_{AA} [67]. The precision of the description of measured jet R_{AA} by a given parameterization is quantified in terms of χ^2 evaluated for 0 – 10% centrality bin and for all centrality bins.

with the results of the analysis of Casimir scaling suggesting $c_F \sim 1.7$ [72]. As alternative values of c_F , we use the value of leading-order approximation, $c_F = C_A/C_F = 9/4$, and the value used in Hybrid model calculations, $c_F = (9/4)^{1/3} \doteq 1.31$, [18].

The default parameterization, which is found to describe the data with the highest accuracy, uses power-law ansatz for the energy loss from Eq. (3), simulation of isospin and nPDFs effects (discussed in Section 3), and parameterization of energy loss fluctuations based on Eq. (8) with parameters determined by fitting the energy loss distribution published in [55]. The comparison of the data and the parameterization is shown in Fig. 2. The power-law parameter is found to be $\alpha = 0.27 \pm 0.03$, $\langle \Delta p_T^{\text{jet}} \rangle_{0-10\%}$ and $\langle \Delta p_T^{\text{jet}} \rangle_{70-80\%}$ were found to be 15.0 ± 0.2 GeV and 1.9 ± 0.1 GeV, respectively.

The default parameterization (labeled ‘p1’) is compared to other parameterizations as summarized in Table 1. Parameterizations p2 and p3 represent alternatives to p1 with $c_F = (9/4)^{1/3}$ and $c_F = 9/4$, respectively. One may see from the table that three parameterizations, p1, p2, and p3, achieve the same precision. This level of precision can be compared with parameterizations p4 and p5 which do not implement nPDF and isospin effects and which are based on PYTHIA8 and HERWIG7, respectively. One may see that the presence of nPDFs improves the description in the most central collisions, where the highest p_T values are reached and where nPDF effects lead to a flattening of the R_{AA} as also shown in previous studies (see e.g. Refs. [73, 74]). The impact of fluctuations is quantified by parameterization p6 where only average energy loss is applied. A significant decrease in the ability to describe the data is seen, providing a model-independent argument for their importance in the description of realistic jet quenching. A worse description of the data is also achieved when using a modified power-law ansatz for the energy loss with logarithmic p_T dependence from Eq. (9), which is done in parameterization p7. While the agreement between a given parameterization and the data may be further improved for all parameterizations by introducing centrality-dependent parameter α , we may conclude that the ansatz with power-law with one centrality-independent parameter in the exponent provides a sufficient description of inclusive jet R_{AA} (see Figure 2 again).

Equipped with the parameterization, we will proceed with a model-independent estimate of path-length dependence of the parton energy loss and provide a simple extrapolation of jet quenching magnitude from lead-lead to oxygen-oxygen collisions.

5 Path length dependence and system size dependence of jet suppression

The path-length (L) dependence of the jet energy loss may be quantified as $\langle \Delta p_T^{\text{jet}} \rangle \sim \langle L \rangle^\delta$ with $\delta = 1, 2$, and 3 employed in baseline calculations of collisional energy loss, pQCD radiative energy loss, and non-perturbative strong coupling models, respectively [4, 75, 76]. During the past ten years, several studies were done aiming to extract the path-length dependence of parton energy loss from the data on charged particle R_{AA} [46, 47, 48, 49]. Large comparative studies [46, 47] which used also data on the elliptic flow led to inconclusive results of $1 \leq \delta \leq 3$. More recent studies [49] and [48] led to $\delta = 1.02$ and $\delta \sim 1.4$ at high- p_T , respectively. These studies rely on various assumptions such as modeling of medium expansion (which was shown to have an impact on observables directly depending on path-length [73]), power-law approximation of input parton yields (which was shown to be inaccurate [50]), or relationship between energy loss of parton shower and measured charged hadron yields. Studies of path-length dependence of parton energy loss based on jet R_{AA} were also performed based on LBT model of jet quenching [54] finding $\delta < 1$.

To extract the path-length dependence of the energy loss, we use parameterizations described in the previous section, which present results on jet quenching modeling with minimal assumptions on the actual jet quenching mechanism. To model the geometry, we assume that the average path length is proportional to the path length estimates given by Glauber model from Ref. [77]. This represents the simplest possible assumption which is however at least partially validated by the measurements of electro-weak boson production [78, 79, 80, 81, 82, 83] confirming good predictive power of the Glauber model. The left panel of Figure 3 shows the fit by power-law parameterization of path-length,

$$\langle \Delta p_T^{\text{jet}} \rangle = c_0 + c_1 \langle L \rangle^\delta, \quad (10)$$

with c_0, c_1 , and δ being free parameters of the fit. The fit is performed for $\langle \Delta p_T^{\text{jet}} \rangle$ evaluated as a function of $\langle L \rangle$ for p1 parameterization. The fit results in $\delta = 2.01 \pm 0.08$, $c_0 = -0.9 \pm 0.3$, and $c_1 = 0.6 \pm 0.1$. While these values are evaluated for the initial jet $p_T = 100$ GeV, the δ parameter remains the same for any choice of jet p_T in the range of 50 – 500 GeV and parameters c_0 and c_1 are consistent within uncertainties in this jet p_T range. Besides the stability, reassuring is also the fact that c_0 is consistent with 0 within three standard deviations, implying no energy loss for $\langle L \rangle = 0$. The right panel of Figure 3 shows δ parameters for parameterizations p1-p5, which all provided a good description of the jet R_{AA} as discussed in the previous section. The δ is plotted as a function of $\langle \Delta p_T^{\text{jet}} \rangle$ in 0 – 10% centrality bin. While one can see from the figure that different jet quenching scenarios provide rather different values of $\langle \Delta p_T^{\text{jet}} \rangle$, and thus different values of jet quenching parameter \hat{q} , which we do not extract from the data, the value of δ is consistent with 2 for all these parameterizations. These results, therefore, strongly support the radiative nature of parton energy loss.

Given this path-length parameterization of energy loss, one may continue exploring the path-length dependence by evaluating jet v_2 . Jet v_2 quantifies the magnitude of azimuthal-angle modulation of jet yields, which is due to the difference between the energy loss of jets traveling in the direction of the interaction plane (“in” direction) and jets traveling in the direction perpendicular to the interaction plane (“out” direction). The former suffer the energy loss over the path-length L_{in} , while the latter suffer the energy loss over the path-length L_{out} . The jet v_2 may then be estimated as [84]

$$v_2 \approx \frac{1}{2} \frac{R_{\text{AA}}(L_{\text{in}}) - R_{\text{AA}}(L_{\text{out}})}{R_{\text{AA}}(L_{\text{in}}) + R_{\text{AA}}(L_{\text{out}})}. \quad (11)$$

To perform basic cross-check, we stay within the Glauber model, which allows us to estimate the average path length traveled in the directions in and out, which differ from the average path length, $\langle L \rangle$, by factors ΔL_{in} and ΔL_{out} , respectively. The L_{in} and L_{out} in Eq. (11) are then given by

$$L_{\text{in}} = \langle L \rangle - c \cdot \Delta L_{\text{in}}, \quad (12)$$

$$L_{\text{out}} = \langle L \rangle + c \cdot \Delta L_{\text{out}}. \quad (13)$$

Since the relative difference between $\langle L \rangle$ and L_{in} or L_{out} may differ in reality from the estimates by the Glauber model due to the expansion of the media, a free parameter c is introduced, which is, however, enforced to be the same for all the centrality bins in this analysis. The $c = 1$ would imply traveling through the medium of the same shape as that given by the Glauber model. The $c < 1$ implies the smearing of the Glauber model shape. The comparison between calculated v_2 and data [85] is shown in the right panel of Figure 4. A good description of the data is found for $c = 0.35$, implying that ΔL_{in} and ΔL_{out} in reality differ roughly by a factor of three from those estimated by

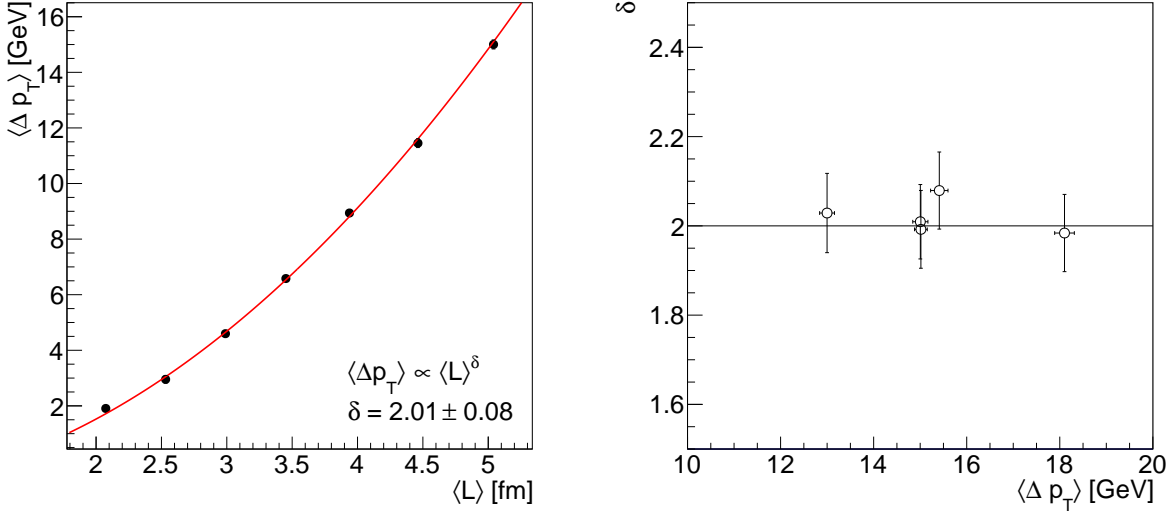


Fig. 3. *Left:* Path-length dependence of average jet energy loss extracted from the data using the parametric model for parameterization p1. *Right:* Power δ of the path-length dependence of jet energy loss (y axis) versus average lost energy (x axis) obtained for parameterizations p1-p5 of the energy loss.

Glauber model. A good description of v_2 is achieved in all published centrality bins except for the bin 0 – 5%, which is found to be consistent with 0 in the data but is calculated to be non-zero in the parametric model. This is likely connected with the presence of a sizable v_3 component, which is measured to be much larger than v_2 , and the formula (11) is therefore expected to fail. This successful description of jet v_2 provides an independent argument in favor of the validity of L^2 dependence of the energy loss that we reported before. The approach used here may also allow relatively simple testing of the impact of different medium profiles on energy loss.

We now turn our attention to the system-size dependence of energy loss. Besides exploring the path-length dependence of parton energy loss, the parameterization of the energy loss may be used to predict the magnitude of jet R_{AA} in upcoming oxygen-oxygen (O+O) collisions. First, the linear extrapolation of the energy loss to 7 TeV is done from $\langle \Delta p_T^{\text{jet}} \rangle$ for 2.76 TeV jet spectra determined in Ref. [51] and $\langle \Delta p_T^{\text{jet}} \rangle$ for 5.02 TeV jets calculated here. The value of $\langle \Delta p_T^{\text{jet}} \rangle$ at 100 GeV is used as a reference value to determine scale factors used to scale the Pb+Pb 5.02 TeV R_{AA} calculations to O+O 7 TeV R_{AA} . The scale factors are determined using parameterizations p1-p3 and they vary from 1.25 to 1.42. The average path lengths in two different percentiles of O+O collisions, namely 0 – 10% and 0 – 70%, are calculated using the Glauber model [77] along with centrality analysis published in Ref. [86]. The above-discussed parameterization of $\langle \Delta p_T^{\text{jet}} \rangle(\langle L \rangle)$ dependence is then used to determine $\langle \Delta p_T^{\text{jet}} \rangle$ in O+O collisions for each of p1-p3. Input jet spectra at 7 TeV were obtained from PYTHIA8 with the same settings as described in Section 3 but with no simulation of nPDF effects. The resulting prediction is shown for 0 – 10% and 0 – 70% O+O collisions in Fig. 4. The band represents the envelope of the results obtained from three parameterizations, p1-p3. One can see that in 0 – 10%, the suppression is significant with the R_{AA} of ≈ 0.76 at $p_T^{\text{jet}} = 50$ GeV. In 0 – 70%, the R_{AA} value is ≈ 0.92 and 0.98 at $p_T^{\text{jet}} = 50$ GeV and $p_T^{\text{jet}} = 300$ GeV, respectively. These results represent a baseline prediction for jet quenching in O+O collisions, which may be seen in the data if the underlying energy loss mechanism is the same in O+O and Pb+Pb collisions in the given kinematic window, if the role of fluctuations is comparable and if nPDF effects have a small impact on the jet R_{AA} .

The last topic we briefly discuss is the parton mass dependence of energy loss. To do that, we repeat the minimization from Sec. 4 using the measurement of b -jets [87]. The parameterization of b -jet spectra uses the large inclusive jet sample described in Section 3. The extracted magnitude of energy loss is then fitted by the power-law path-length dependence of the energy loss (Eq.(10)) resulting in parameter $\delta = 2.6 \pm 1.6$. This is further compared with the energy loss extracted from the R_{AA} of $R = 0.2$ jets leading to $\delta = 1.9 \pm 0.4$. Both values are, therefore, consistent with each other within the uncertainties, and one can conclude that the current precision of b -jet measurement does not provide sufficient precision to discriminate expected differences [88, 89, 90, 91] in the path-length dependence of energy loss between inclusive jets and b -jets. To address this in the future, it is especially important to measure the suppression in more centrality bins since, for fewer centrality bins, the precision of extracted δ significantly decreases, as can be seen if one compares the precision of previously extracted δ value for $R = 0.4$ jets and the value for $R = 0.2$ jets ($\delta = 2.01 \pm 0.08$ and $\delta = 1.9 \pm 0.4$, respectively).

We will now turn our attention to gaining insights on the jet suppression in γ -jet events.

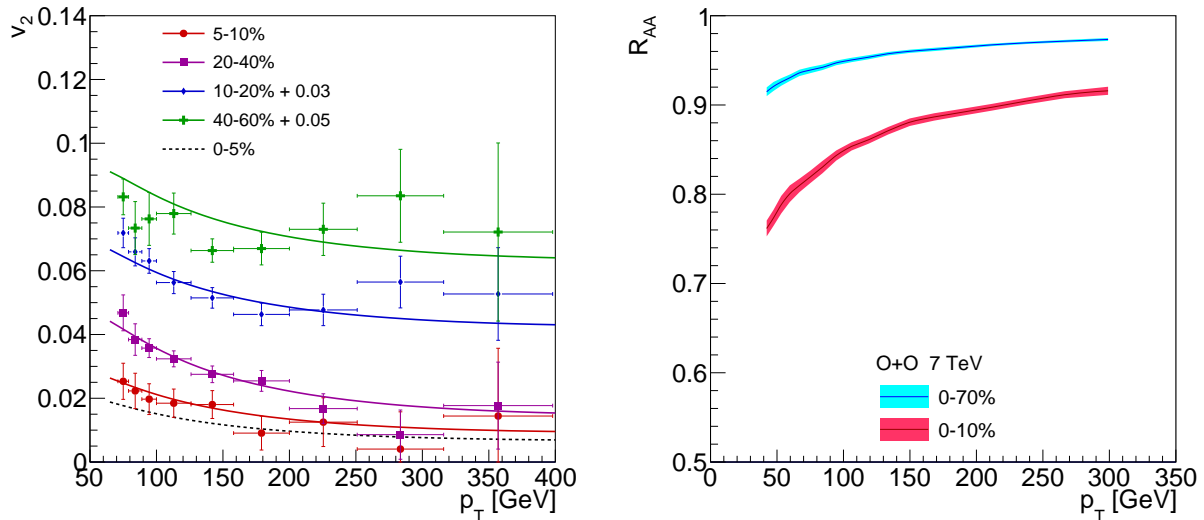


Fig. 4. *Left:* Jet v_2 determined using the parameterization of path-length dependence of inclusive jet suppression (lines) compared with measured jet v_2 [85] (data points). *Right:* Prediction of jet R_{AA} distributions for 7 TeV oxygen-oxygen collisions using parameterizations of inclusive jet suppression at 2.76 TeV and 5.02 TeV.

6 Suppression of jets in γ -jet system

Having in hand parameters describing well the suppression of inclusive jets, we may proceed with applying the suppression on jets in the γ -jet system. First, we use the reweighted PYTHIA8 jet spectra with nPDFs as described in Sec. 3 and calculate the R_{AA} for the quenching parameterizations p1-p3 which employ three different values of c_F and which all describe the inclusive jet R_{AA} data with the same precision. To calculate the R_{AA} in centrality bins of the published measurement [35], we use the Glauber model to estimate the average path length for those centrality bins and the above-given parameterization of $\langle \Delta p_T^{\text{jet}} \rangle (\langle L \rangle)$ dependence. The result of the calculations is shown together with the measured R_{AA} in the upper left panel of Figure 5. One can see that the differences in R_{AA} between different c_F values are rather large, confirming that the γ -jet measurement can help constrain the role of flavor in the jet quenching. One can also see that the calculated R_{AA} qualitatively reproduces the shape of the measured R_{AA} in the region of $p_T^{\text{jet}} \lesssim 120$ GeV. Namely, it reproduces the decrease of R_{AA} at low p_T^{jet} , a presence of minimum, and then a smooth rise with increasing p_T . None of the quenching parameterizations used in the previous section can, however, reproduce the local maximum present in the data at $p_T^{\text{jet}} \approx 150$ GeV and the subsequent decrease. Since this local maximum is present for all the centralities, we may speculate that this increase is connected with fluctuations in the pp reference ¹. While the parametric modeling can describe quite successfully the shape of the measured R_{AA} , especially in central collisions, it noticeably fails in describing the overall magnitude of R_{AA} in 0 – 10% and 10 – 30% centrality bins.

To further explore the building blocks needed to reproduce the measured R_{AA} we evaluate the R_{AA} for the same jet quenching parameters but different input spectra of jets in the γ -jet system. We compare the following inputs: PYTHIA8 with no reweighting applied to match the MC jet spectra to those measured in the pp data; PYTHIA8 with reweighting applied only on direct photons; PYTHIA8 with reweighting applied only on photons from fragmentation; PYTHIA8 with no nPDFs (all previously described versions apply nPDFs for the spectra entering the numerator of R_{AA}); and HERWIG7 with no nPDFs. A comparison of the five calculated R_{AA} distributions is shown in the upper right panel of Figure 5. One can see that reweighting of jet spectra to match those measured in the data influences the magnitude of the calculated R_{AA} by less than 10% (and slightly more in the case of HERWIG, which we do not show). Implementation of nPDF effects influences the magnitude of R_{AA} more substantially, by 15-20%. The choice of MC generator (PYTHIA8 vs HERWIG7) influences the magnitude of R_{AA} by another $\approx 10\%$. We may, therefore, conclude that the precise knowledge of input parton spectra plays an important role in the ability to determine the exact shape of R_{AA} . At the same time, the lack of full knowledge of input parton spectra cannot fully explain the difference in the magnitude of R_{AA} among different centrality classes.

¹ The presence of this local maximum is not significant with respect to uncertainties delivered by the experiment. Nevertheless, it is also interesting to notice that Figure 1 in Ref. [35] contains a fluctuation in quark jet fraction in PYTHIA8 in a similar p_T^{jet} window. Such fluctuation in MC reference could, in principle, affect, e.g., the unfolding of the data.

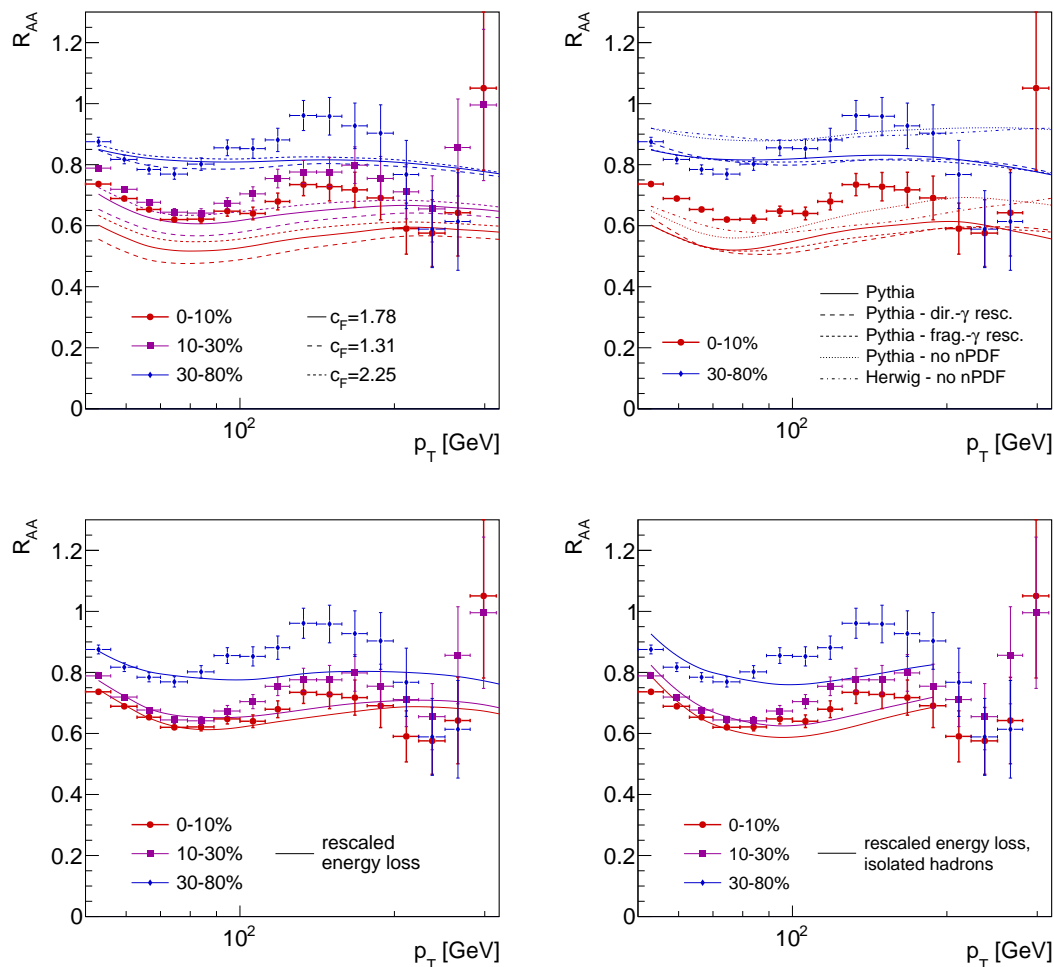


Fig. 5. Jet R_{AA} measured in the γ -jet system [35] (data points) compared with various setup of the parametric modelling (lines): different choice of color factor (upper left), different choice of input jet spectra (upper right), magnitude of the energy loss rescaled compared to the inclusive energy loss (lower left). Lower right panel shows jet R_{AA} evaluated for jets from the isolated-hadron-jet system.

A possible source of the apparently smaller magnitude of the energy loss suffered by jets in the γ -jet system than in the inclusive jet system may be the selection bias [92,93]. Both jets in the dijet system, which dominates the inclusive jet sample, suffer the energy loss, while in the case of the γ -jets, it is only one jet that interacts with the medium, whereas the γ remains unresolved by the medium. We will not attempt to model the selection bias here. We will only quantify the change in the average path length needed to achieve a good description of the measured R_{AA} . This is done by minimizing differences between the model and the data while changing the magnitude of the quenching dictated by parameter s . We can then translate this change to a change in the average path-length traveled by jets in the case of γ -jet events, $\langle L_\gamma \rangle$ and average path-length traveled in the case of inclusive jet events, $\langle L \rangle$. The $\langle L_\gamma \rangle / \langle L \rangle$ ratios are found to be the following: 0.80 ± 0.02 , 0.9 ± 0.03 , and 1.07 ± 0.03 for 0 – 10%, 10 – 30%, and 30 – 80% centrality collisions, respectively. This R_{AA} is then shown in the lower left panel of Figure 5. One can see a good model-to-data agreement for the R_{AA} region outside of the second maximum. The above-calculated ratios may then be valuable for constraining models implementing the differences between the inclusive jet suppression and γ -jet suppression at the microscopic level.

While the change in the path-length dependence of energy loss may be an acceptable source of the unexpected centrality dependence of the energy loss in γ -jet events, it is also useful to discuss plausible contamination of signal by the inclusive jet background. The ratio of γ -jet to inclusive jet cross-sections determined from pp data [35] is $\approx 2.5 \cdot 10^{-4}$ for jets with $50 < p_T < 100$ GeV. This large factor brings a question if the photon selection could be contaminated by isolated, predominantly neutral hadrons that could mimic a photon. While experiments always perform sophisticated shower-shape cuts and other procedures to eliminate these backgrounds, and they quantify residual contributions in

systematic uncertainties, we found it useful to provide quantitative insight into this component. To achieve that, we use the large sample of PYTHIA dijet events (described in Sec. 3) to find the cross-section for the production of jets opposite isolated hadrons with $p_T > 50$ GeV. The isolation criteria are the same as those applied previously on photons (described in Sec. 3). The ratio of the cross-section for producing the jet with $50 < p_T < 100$ GeV in the sample with isolated hadrons and in the inclusive jet sample is found to be $1.4 \cdot 10^{-4}$ and $5.6 \cdot 10^{-5}$ for isolated hadrons of any charge and for predominately neutral hadrons, respectively. Predominately neutral hadrons are a mixture of neutral hadrons and charged hadrons that are simulated to be missed by tracking due to finite charged-particle reconstruction efficiency (here taken to be 80% [94]). Given the uncertainty of PYTHIA to model the very end of the fragmentation spectrum and given the fact that these cross-sections are of a similar order of magnitude as those for the measured cross-section of jets in the γ -jet system, we conclude that the contamination by inclusive jets remains plausible. Its validity is to be judged by individual experiments. It is now important to evaluate the jet R_{AA} for jets in the isolated-hadron-jet system. The resulting R_{AA} is shown in the lower right panel of Figure 5. In that evaluation, we fixed the values of α and c_F coefficients to be the same as in the main study and only optimized values of s parameter by the same minimization procedure as the one used before. One can see that the shape of the resulting R_{AA} is strikingly similar to that obtained for jets from the γ -jet system.

7 Summary and conclusions

The parametric approach to the jet quenching modeling was used to study jet quenching in inclusive jet, b -jet, and γ -jet systems. Various parameterizations of p_T^{jet} dependence of energy loss were studied, and it was shown that a parameterization with implemented isospin and nPDF effects, energy loss fluctuations, and pure power-law ansatz for p_T^{jet} -dependence of the energy loss provides the best description of inclusive jet R_{AA} . The power-law index α in $(p_T^{\text{jet}})^\alpha$ dependence of energy loss was found to be centrality independent with a value of 0.27 ± 0.03 for color factor $c_F = 1.78$. Using parameterizations of inclusive jet suppression, the path-length (L) dependence of energy loss was quantified under the assumption that the average in-medium path length in different centrality bins is proportional to that provided by the Glauber model. The power-law index δ in L^δ dependence of energy loss was found to be 2.01 ± 0.08 for the parameterization which provided the best description of inclusive jet R_{AA} . For all other well-performing parameterizations, the path-length dependence was also found to be consistent with L^2 . These results thus strongly support the radiative nature of parton energy loss. Using these parameterizations, measured jet v_2 was reproduced, and a prediction of the expected magnitude of jet R_{AA} in 7 TeV oxygen-oxygen collisions was made. The b -jet suppression was also briefly studied, showing statistically insignificant differences in the path-length dependence with respect to the inclusive jet suppression.

The p_T^{jet} and path-length parameterizations of the energy loss were then used to study the jet suppression in the γ -jet system. It was shown that the differences between the suppression of quark-initiated and gluon-initiated jets may explain the shape of the R_{AA} of jets in the γ -jet system in all centrality bins and its magnitude in the centrality bin of 30 – 80%, but more detailed knowledge of jet quenching at the microscopic level is needed to understand the apparent lack of suppression in 0 – 10% and 10 – 30% central collisions. A firm understanding of inclusive jet backgrounds is also important.

Since the parametric approach used in this paper represents a framework with only minimal assumptions on the underlying jet-quenching mechanism, the provided results may serve as a benchmark for microscopic models of parton energy loss in expanding quark-gluon plasma. The presented work also demonstrates a way to further study the impact of various aspects of jet quenching physics on measured data.

Acknowledgments

This work was supported by The Ministry of Education, Youth and Sports of the Czech Republic under project ERC-CZ LL2327.

References

1. H.-T. Ding, F. Karsch, S. Mukherjee, Thermodynamics of strong-interaction matter from Lattice QCD, *Int. J. Mod. Phys. E* 24 (10) (2015) 1530007. [arXiv:1504.05274](https://arxiv.org/abs/1504.05274), [doi:10.1142/S0218301315300076](https://doi.org/10.1142/S0218301315300076).
2. W. Busza, K. Rajagopal, W. van der Schee, Heavy Ion Collisions: The Big Picture, and the Big Questions, *Ann. Rev. Nucl. Part. Sci.* 68 (2018) 339–376. [arXiv:1802.04801](https://arxiv.org/abs/1802.04801), [doi:10.1146/annurev-nucl-101917-020852](https://doi.org/10.1146/annurev-nucl-101917-020852).
3. Y. Mehtar-Tani, J. G. Milhano, K. Tywoniuk, Jet physics in heavy-ion collisions, *Int. J. Mod. Phys. A* 28 (2013) 1340013. [arXiv:1302.2579](https://arxiv.org/abs/1302.2579), [doi:10.1142/S0217751X13400137](https://doi.org/10.1142/S0217751X13400137).

4. A. Majumder, M. Van Leeuwen, The Theory and Phenomenology of Perturbative QCD Based Jet Quenching, *Prog. Part. Nucl. Phys.* 66 (2011) 41–92. [arXiv:1002.2206](#), [doi:10.1016/j.pnnp.2010.09.001](#).
5. J. Casalderrey-Solana, C. A. Salgado, Introductory lectures on jet quenching in heavy ion collisions, *Acta Phys. Polon. B* 38 (2007) 3731–3794. [arXiv:0712.3443](#).
6. S. Cao, X.-N. Wang, Jet quenching and medium response in high-energy heavy-ion collisions: a review, *Rept. Prog. Phys.* 84 (2) (2021) 024301. [arXiv:2002.04028](#), [doi:10.1088/1361-6633/abc22b](#).
7. L. Apolinário, Y.-J. Lee, M. Winn, Heavy quarks and jets as probes of the QGP, *Prog. Part. Nucl. Phys.* 127 (2022) 103990. [arXiv:2203.16352](#), [doi:10.1016/j.pnnp.2022.103990](#).
8. L. Cunqueiro, A. M. Sickles, Studying the QGP with Jets at the LHC and RHIC, *Prog. Part. Nucl. Phys.* 124 (2022) 103940. [arXiv:2110.14490](#), [doi:10.1016/j.pnnp.2022.103940](#).
9. M. Connors, C. Nattrass, R. Reed, S. Salur, Jet measurements in heavy ion physics, *Rev. Mod. Phys.* 90 (2018) 025005. [arXiv:1705.01974](#), [doi:10.1103/RevModPhys.90.025005](#).
10. Z. Citron, et al., Report from Working Group 5: Future physics opportunities for high-density QCD at the LHC with heavy-ion and proton beams, CERN Yellow Rep. Monogr. 7 (2019) 1159–1410. [arXiv:1812.06772](#), [doi:10.23731/CYRM-2019-007.1159](#).
11. G. Dissertori, I. G. Knowles, M. Schmelling, *Quantum Chromodynamics: High energy experiments and theory*, Oxford University Press, 2009. [doi:10.1093/acprof:oso/9780199566419.001.0001](#).
12. J. Gallicchio, M. D. Schwartz, Quark and Gluon Tagging at the LHC, *Phys. Rev. Lett.* 107 (2011) 172001. [arXiv:1106.3076](#), [doi:10.1103/PhysRevLett.107.172001](#).
13. Y. Mehtar-Tani, S. Schlichting, Universal quark to gluon ratio in medium-induced parton cascade, *JHEP* 09 (2018) 144. [arXiv:1807.06181](#), [doi:10.1007/JHEP09\(2018\)144](#).
14. Y.-T. Chien, I. Vitev, Towards the understanding of jet shapes and cross sections in heavy ion collisions using soft-collinear effective theory, *JHEP* 05 (2016) 023. [arXiv:1509.07257](#), [doi:10.1007/JHEP05\(2016\)023](#).
15. J. Casalderrey-Solana, D. C. Gulhan, J. G. Milhano, D. Pablos, K. Rajagopal, Predictions for Boson-Jet Observables and Fragmentation Function Ratios from a Hybrid Strong/Weak Coupling Model for Jet Quenching, *JHEP* 03 (2016) 053. [arXiv:1508.00815](#), [doi:10.1007/JHEP03\(2016\)053](#).
16. K. Zapp, G. Ingelman, J. Rathsman, J. Stachel, U. A. Wiedemann, A Monte Carlo Model for 'Jet Quenching', *Eur. Phys. J. C* 60 (2009) 617–632. [arXiv:0804.3568](#), [doi:10.1140/epjc/s10052-009-0941-2](#).
17. N. Armesto, L. Cunqueiro, C. A. Salgado, Q-PYTHIA: A Medium-modified implementation of final state radiation, *Eur. Phys. J. C* 63 (2009) 679–690. [arXiv:0907.1014](#), [doi:10.1140/epjc/s10052-009-1133-9](#).
18. J. Casalderrey-Solana, D. C. Gulhan, J. G. Milhano, D. Pablos, K. Rajagopal, A Hybrid Strong/Weak Coupling Approach to Jet Quenching, *JHEP* 10 (2014) 019, [Erratum: *JHEP* 09, 175 (2015)]. [arXiv:1405.3864](#), [doi:10.1007/JHEP09\(2015\)175](#).
19. B. Schenke, C. Gale, S. Jeon, MARTINI: An Event generator for relativistic heavy-ion collisions, *Phys. Rev. C* 80 (2009) 054913. [arXiv:0909.2037](#), [doi:10.1103/PhysRevC.80.054913](#).
20. A. Majumder, Incorporating Space-Time Within Medium-Modified Jet Event Generators, *Phys. Rev. C* 88 (2013) 014909. [arXiv:1301.5323](#), [doi:10.1103/PhysRevC.88.014909](#).
21. X.-N. Wang, Y. Zhu, Medium Modification of γ -jets in High-energy Heavy-ion Collisions, *Phys. Rev. Lett.* 111 (6) (2013) 062301. [arXiv:1302.5874](#), [doi:10.1103/PhysRevLett.111.062301](#).
22. Y. Mehtar-Tani, C. A. Salgado, K. Tywoniuk, Anti-angular ordering of gluon radiation in QCD media, *Phys. Rev. Lett.* 106 (2011) 122002. [arXiv:1009.2965](#), [doi:10.1103/PhysRevLett.106.122002](#).
23. J. Casalderrey-Solana, Y. Mehtar-Tani, C. A. Salgado, K. Tywoniuk, New picture of jet quenching dictated by color coherence, *Phys. Lett. B* 725 (2013) 357–360. [arXiv:1210.7765](#), [doi:10.1016/j.physletb.2013.07.046](#).
24. Y. Mehtar-Tani, C. A. Salgado, K. Tywoniuk, Jets in QCD Media: From Color Coherence to Decoherence, *Phys. Lett. B* 707 (2012) 156–159. [arXiv:1102.4317](#), [doi:10.1016/j.physletb.2011.12.042](#).
25. Y. Mehtar-Tani, K. Tywoniuk, Jet coherence in QCD media: the antenna radiation spectrum, *JHEP* 01 (2013) 031. [arXiv:1105.1346](#), [doi:10.1007/JHEP01\(2013\)031](#).
26. L. Apolinário, N. Armesto, J. G. Milhano, C. A. Salgado, Medium-induced gluon radiation and colour decoherence beyond the soft approximation, *JHEP* 02 (2015) 119. [arXiv:1407.0599](#), [doi:10.1007/JHEP02\(2015\)119](#).
27. Y. Mehtar-Tani, K. Tywoniuk, Sudakov suppression of jets in QCD media, *Phys. Rev. D* 98 (5) (2018) 051501. [arXiv:1707.07361](#), [doi:10.1103/PhysRevD.98.051501](#).
28. J. a. Barata, F. Domínguez, C. A. Salgado, V. Vila, A modified in-medium evolution equation with color coherence, *JHEP* 05 (2021) 148. [arXiv:2101.12135](#), [doi:10.1007/JHEP05\(2021\)148](#).
29. P. Caucal, E. Iancu, G. Soyez, Deciphering the z_g distribution in ultrarelativistic heavy ion collisions, *JHEP* 10 (2019) 273. [arXiv:1907.04866](#), [doi:10.1007/JHEP10\(2019\)273](#).
30. A. Kumar, et al., Inclusive jet and hadron suppression in a multistage approach, *Phys. Rev. C* 107 (3) (2023) 034911. [arXiv:2204.01163](#), [doi:10.1103/PhysRevC.107.034911](#).
31. L. Cunqueiro, D. Pablos, A. Soto-Ontoso, M. Spousta, A. Takacs, M. Verweij, Isolating perturbative QCD splittings in heavy-ion collisions (11 2023). [arXiv:2311.07643](#).
32. P. Caucal, E. Iancu, A. H. Mueller, G. Soyez, Vacuum-like jet fragmentation in a dense QCD medium, *Phys. Rev. Lett.* 120 (2018) 232001. [arXiv:1801.09703](#), [doi:10.1103/PhysRevLett.120.232001](#).
33. D. Pablos, A. Soto-Ontoso, Pushing forward jet substructure measurements in heavy-ion collisions, *Phys. Rev. D* 107 (9) (2023) 094003. [arXiv:2210.07901](#), [doi:10.1103/PhysRevD.107.094003](#).

34. X.-N. Wang, Z. Huang, I. Sarcevic, Jet quenching in the opposite direction of a tagged photon in high-energy heavy ion collisions, *Phys. Rev. Lett.* 77 (1996) 231–234. [arXiv:hep-ph/9605213](#), [doi:10.1103/PhysRevLett.77.231](#).
35. ATLAS Collaboration, Comparison of inclusive and photon-tagged jet suppression in 5.02 TeV Pb+Pb collisions with ATLAS, *Phys. Lett. B* 846 (2023) 138154. [arXiv:2303.10090](#), [doi:10.1016/j.physletb.2023.138154](#).
36. CMS Collaboration, Studies of Jet Quenching using Isolated-Photon + Jet Correlations in PbPb and *pp* Collisions at $\sqrt{s_{NN}} = 2.76$ TeV, *Phys. Lett. B* 718 (2013) 773–794. [arXiv:1205.0206](#), [doi:10.1016/j.physletb.2012.11.003](#).
37. CMS Collaboration, Study of jet quenching with isolated-photon+jet correlations in PbPb and *pp* collisions at $\sqrt{s_{NN}} = 5.02$ TeV, *Phys. Lett. B* 785 (2018) 14–39. [arXiv:1711.09738](#), [doi:10.1016/j.physletb.2018.07.061](#).
38. CMS Collaboration, Jet Shapes of Isolated Photon-Tagged Jets in Pb-Pb and *pp* Collisions at $\sqrt{s_{NN}} = 5.02$ TeV, *Phys. Rev. Lett.* 122 (15) (2019) 152001. [arXiv:1809.08602](#), [doi:10.1103/PhysRevLett.122.152001](#).
39. CMS Collaboration, Observation of Medium-Induced Modifications of Jet Fragmentation in Pb-Pb Collisions at $\sqrt{s_{NN}} = 5.02$ TeV Using Isolated Photon-Tagged Jets, *Phys. Rev. Lett.* 121 (24) (2018) 242301. [arXiv:1801.04895](#), [doi:10.1103/PhysRevLett.121.242301](#).
40. ATLAS Collaboration, Measurement of photon-jet transverse momentum correlations in 5.02 TeV Pb+Pb and *pp* collisions with ATLAS, *Phys. Lett. B* 789 (2019) 167–190. [arXiv:1809.07280](#), [doi:10.1016/j.physletb.2018.12.023](#).
41. ATLAS Collaboration, Comparison of Fragmentation Functions for Jets Dominated by Light Quarks and Gluons from *pp* and Pb+Pb Collisions in ATLAS, *Phys. Rev. Lett.* 123 (4) (2019) 042001. [arXiv:1902.10007](#), [doi:10.1103/PhysRevLett.123.042001](#).
42. Liu, A et al., ALICE Collaboration, Isolated Photon-Jet Correlations in Pb-Pb Collisions at $\sqrt{s_{NN}} = 5.02$ TeV in ALICE, *Acta Phys. Polon. Supp.* 16 (1) (2023) 1–A54. [arXiv:2208.08523](#), [doi:10.5506/APhysPolBSupp.16.1-A54](#).
43. H. Zhang, J. F. Owens, E. Wang, X.-N. Wang, Tomography of high-energy nuclear collisions with photon-hadron correlations, *Phys. Rev. Lett.* 103 (2009) 032302. [arXiv:0902.4000](#), [doi:10.1103/PhysRevLett.103.032302](#).
44. G.-Y. Qin, J. Ruppert, C. Gale, S. Jeon, G. D. Moore, Jet energy loss, photon production, and photon-hadron correlations at RHIC, *Phys. Rev. C* 80 (2009) 054909. [arXiv:0906.3280](#), [doi:10.1103/PhysRevC.80.054909](#).
45. T. Renk, Towards jet tomography: gamma-hadron correlations, *Phys. Rev. C* 74 (2006) 034906. [arXiv:hep-ph/0607166](#), [doi:10.1103/PhysRevC.74.034906](#).
46. B. Betz, M. Gyulassy, Constraints on the Path-Length Dependence of Jet Quenching in Nuclear Collisions at RHIC and LHC, *JHEP* 08 (2014) 090, [Erratum: *JHEP* 10, 043 (2014)]. [arXiv:1404.6378](#), [doi:10.1007/JHEP10\(2014\)043](#).
47. B. Betz, M. Gyulassy, M. Luzum, J. Noronha, J. Noronha-Hostler, I. Portillo, C. Ratti, Cumulants and nonlinear response of high p_T harmonic flow at $\sqrt{s_{NN}} = 5.02$ TeV, *Phys. Rev. C* 95 (4) (2017) 044901. [arXiv:1609.05171](#), [doi:10.1103/PhysRevC.95.044901](#).
48. M. Djordjevic, D. Zigic, M. Djordjevic, J. Auvinen, How to test path-length dependence in energy loss mechanisms: analysis leading to a new observable, *Phys. Rev. C* 99 (6) (2019) 061902. [arXiv:1805.04030](#), [doi:10.1103/PhysRevC.99.061902](#).
49. F. Arleo, G. Falmagne, Probing the path-length dependence of parton energy loss via scaling properties in heavy ion collisions, *Phys. Rev. D* 109 (5) (2024) L051503. [arXiv:2212.01324](#), [doi:10.1103/PhysRevD.109.L051503](#).
50. M. Spousta, B. Cole, Interpreting single jet measurements in Pb + Pb collisions at the LHC, *Eur. Phys. J. C* 76 (2) (2016) 50. [arXiv:1504.05169](#), [doi:10.1140/epjc/s10052-016-3896-0](#).
51. M. Spousta, On similarity of jet quenching and charmonia suppression, *Phys. Lett. B* 767 (2017) 10–15. [arXiv:1606.00903](#), [doi:10.1016/j.physletb.2017.01.041](#).
52. Y. He, L.-G. Pang, X.-N. Wang, Bayesian extraction of jet energy loss distributions in heavy-ion collisions, *Phys. Rev. Lett.* 122 (25) (2019) 252302. [arXiv:1808.05310](#), [doi:10.1103/PhysRevLett.122.252302](#).
53. Y. He, S. Cao, W. Chen, T. Luo, L.-G. Pang, X.-N. Wang, Interplaying mechanisms behind single inclusive jet suppression in heavy-ion collisions, *Phys. Rev. C* 99 (5) (2019) 054911. [arXiv:1809.02525](#), [doi:10.1103/PhysRevC.99.054911](#).
54. J. Wu, W. Ke, X.-N. Wang, Bayesian inference of the path-length dependence of jet energy loss, *Phys. Rev. C* 108 (3) (2023) 034911. [arXiv:2304.06339](#), [doi:10.1103/PhysRevC.108.034911](#).
55. J. Brewer, Q. Brodsky, K. Rajagopal, Disentangling jet modification in jet simulations and in Z+jet data, *JHEP* 02 (2022) 175. [arXiv:2110.13159](#), [doi:10.1007/JHEP02\(2022\)175](#).
56. T. Sjöstrand, S. Ask, J. R. Christiansen, R. Corke, N. Desai, P. Ilten, S. Mrenna, S. Prestel, C. O. Rasmussen, P. Z. Skands, An introduction to PYTHIA 8.2, *Comput. Phys. Commun.* 191 (2015) 159–177. [arXiv:1410.3012](#), [doi:10.1016/j.cpc.2015.01.024](#).
57. C. Bierlich, et al., A comprehensive guide to the physics and usage of PYTHIA 8.3 (3 2022). [arXiv:2203.11601](#), [doi:10.21468/SciPostPhysCodeb.8](#).
58. ATLAS Collaboration, ATLAS Pythia 8 tunes to 7 TeV data (11 2014).
59. R. D. Ball, et al., Parton distributions with LHC data, *Nucl. Phys. B* 867 (2013) 244–289. [arXiv:1207.1303](#), [doi:10.1016/j.nuclphysb.2012.10.003](#).
60. ATLAS Collaboration, Measurement of suppression of large-radius jets and its dependence on substructure in Pb+Pb collisions at $\sqrt{s_{NN}} = 5.02$ TeV with the ATLAS detector (1 2023). [arXiv:2301.05606](#).
61. M. Bahr, et al., Herwig++ Physics and Manual, *Eur. Phys. J. C* 58 (2008) 639–707. [arXiv:0803.0883](#), [doi:10.1140/epjc/s10052-008-0798-9](#).
62. ATLAS Collaboration, Jet energy scale and resolution measured in proton–proton collisions at $\sqrt{s} = 13$ TeV with the ATLAS detector, *Eur. Phys. J. C* 81 (8) (2021) 689. [arXiv:2007.02645](#), [doi:10.1140/epjc/s10052-021-09402-3](#).
63. CMS Collaboration, Jet energy scale and resolution in the CMS experiment in *pp* collisions at 8 TeV, *JINST* 12 (02) (2017) P02014. [arXiv:1607.03663](#), [doi:10.1088/1748-0221/12/02/P02014](#).

64. M. Cacciari, G. P. Salam, G. Soyez, The anti- k_t jet clustering algorithm, JHEP 04 (2008) 063. [arXiv:0802.1189](#), [doi:10.1088/1126-6708/2008/04/063](#).
65. M. Cacciari, G. P. Salam, G. Soyez, FastJet User Manual, Eur. Phys. J. C 72 (2012) 1896. [arXiv:1111.6097](#), [doi:10.1140/epjc/s10052-012-1896-2](#).
66. L. A. Harland-Lang, A. D. Martin, P. Motylinski, R. S. Thorne, Parton distributions in the lhc era: Mmht 2014 pdfs, The European Physical Journal C 75 (5) (May 2015). [doi:10.1140/epjc/s10052-015-3397-6](#). URL <http://dx.doi.org/10.1140/epjc/s10052-015-3397-6>
67. M. Aaboud, et al., Measurement of the nuclear modification factor for inclusive jets in Pb+Pb collisions at $\sqrt{s_{NN}} = 5.02$ TeV with the ATLAS detector, Phys. Lett. B 790 (2019) 108–128. [arXiv:1805.05635](#), [doi:10.1016/j.physletb.2018.10.076](#).
68. K. J. Eskola, P. Paakkinen, H. Paukkunen, C. A. Salgado, EPPS16: Nuclear parton distributions with LHC data, Eur. Phys. J. C 77 (3) (2017) 163. [arXiv:1612.05741](#), [doi:10.1140/epjc/s10052-017-4725-9](#).
69. F. James, M. Roos, Minuit: A System for Function Minimization and Analysis of the Parameter Errors and Correlations, Comput. Phys. Commun. 10 (1975) 343–367. [doi:10.1016/0010-4655\(75\)90039-9](#).
70. A. Capella, I. M. Dremin, J. W. Gary, V. A. Nechitailo, J. Tran Thanh Van, Evolution of average multiplicities of quark and gluon jets, Phys. Rev. D61 (2000) 074009. [arXiv:hep-ph/9910226](#), [doi:10.1103/PhysRevD.61.074009](#).
71. D. Acosta, et al., Measurement of charged particle multiplicities in gluon and quark jets in $p\bar{p}$ collisions at $\sqrt{s} = 1.8$ TeV, Phys. Rev. Lett. 94 (2005) 171802. [doi:10.1103/PhysRevLett.94.171802](#).
72. L. Apolinário, J. a. Barata, G. Milhano, On the breaking of Casimir scaling in jet quenching, Eur. Phys. J. C 80 (6) (2020) 586. [arXiv:2003.02893](#), [doi:10.1140/epjc/s10052-020-8133-1](#).
73. S. P. Adhya, C. A. Salgado, M. Spousta, K. Tywoniuk, Multi-partonic medium induced cascades in expanding media, Eur. Phys. J. C 82 (1) (2022) 20. [arXiv:2106.02592](#), [doi:10.1140/epjc/s10052-021-09950-8](#).
74. D. Pablos, Jet Suppression From a Small to Intermediate to Large Radius, Phys. Rev. Lett. 124 (5) (2020) 052301. [arXiv:1907.12301](#), [doi:10.1103/PhysRevLett.124.052301](#).
75. R. Baier, Y. L. Dokshitzer, A. H. Mueller, S. Peigne, D. Schiff, Radiative energy loss of high-energy quarks and gluons in a finite volume quark - gluon plasma, Nucl. Phys. B 483 (1997) 291–320. [arXiv:hep-ph/9607355](#), [doi:10.1016/S0550-3213\(96\)00553-6](#).
76. S. S. Gubser, D. R. Gulotta, S. S. Pufu, F. D. Rocha, Gluon energy loss in the gauge-string duality, JHEP 10 (2008) 052. [arXiv:0803.1470](#), [doi:10.1088/1126-6708/2008/10/052](#).
77. C. Loizides, J. Kamin, D. d’Enterria, Improved Monte Carlo Glauber predictions at present and future nuclear colliders, Phys. Rev. C 97 (5) (2018) 054910, [Erratum: Phys.Rev.C 99, 019901 (2019)]. [arXiv:1710.07098](#), [doi:10.1103/PhysRevC.97.054910](#).
78. ATLAS Collaboration, Centrality, rapidity and transverse momentum dependence of isolated prompt photon production in lead-lead collisions at $\sqrt{s_{NN}} = 2.76$ TeV measured with the ATLAS detector, Phys. Rev. C 93 (3) (2016) 034914. [arXiv:1506.08552](#), [doi:10.1103/PhysRevC.93.034914](#).
79. CMS Collaboration, The production of isolated photons in PbPb and pp collisions at $\sqrt{s_{NN}} = 5.02$ TeV, JHEP 07 (2020) 116. [arXiv:2003.12797](#), [doi:10.1007/JHEP07\(2020\)116](#).
80. ATLAS Collaboration, Measurement of W^\pm boson production in Pb+Pb collisions at $\sqrt{s_{NN}} = 5.02$ TeV with the ATLAS detector, Eur. Phys. J. C 79 (11) (2019) 935. [arXiv:1907.10414](#), [doi:10.1140/epjc/s10052-019-7439-3](#).
81. CMS Collaboration, Study of W Boson Production in PbPb and pp Collisions at $\sqrt{s_{NN}} = 2.76$ TeV, Phys. Lett. B 715 (2012) 66–87. [arXiv:1205.6334](#), [doi:10.1016/j.physletb.2012.07.025](#).
82. ATLAS Collaboration, Z boson production in Pb+Pb collisions at $\sqrt{s_{NN}} = 5.02$ TeV measured by the ATLAS experiment, Phys. Lett. B 802 (2020) 135262. [arXiv:1910.13396](#), [doi:10.1016/j.physletb.2020.135262](#).
83. CMS Collaboration, Study of Z production in PbPb and pp collisions at $\sqrt{s_{NN}} = 2.76$ TeV in the dimuon and dielectron decay channels, JHEP 03 (2015) 022. [arXiv:1410.4825](#), [doi:10.1007/JHEP03\(2015\)022](#).
84. D. Zigic, I. Salom, J. Auvinen, M. Djordjevic, M. Djordjevic, DREENA-C framework: joint R_{AA} and v_2 predictions and implications to QGP tomography, J. Phys. G 46 (8) (2019) 085101. [arXiv:1805.03494](#), [doi:10.1088/1361-6471/ab2356](#).
85. ATLAS Collaboration, Measurements of azimuthal anisotropies of jet production in Pb+Pb collisions at $\sqrt{s_{NN}} = 5.02$ TeV with the ATLAS detector, Phys. Rev. C 105 (6) (2022) 064903. [arXiv:2111.06606](#), [doi:10.1103/PhysRevC.105.064903](#).
86. D. Behera, N. Mallick, S. Tripathy, S. Prasad, A. N. Mishra, R. Sahoo, Predictions on global properties in O+O collisions at the Large Hadron Collider using a multi-phase transport model, Eur. Phys. J. A 58 (9) (2022) 175. [arXiv:2110.04016](#), [doi:10.1140/epja/s10050-022-00823-6](#).
87. ATLAS Collaboration, Measurement of the nuclear modification factor of b -jets in 5.02 TeV Pb+Pb collisions with the ATLAS detector, Eur. Phys. J. C 83 (5) (2023) 438. [arXiv:2204.13530](#), [doi:10.1140/epjc/s10052-023-11427-9](#).
88. D. Zigic, I. Salom, J. Auvinen, M. Djordjevic, M. Djordjevic, DREENA-B framework: first predictions of R_{AA} and v_2 within dynamical energy loss formalism in evolving QCD medium, Phys. Lett. B 791 (2019) 236–241. [arXiv:1805.04786](#), [doi:10.1016/j.physletb.2019.02.020](#).
89. Y. L. Dokshitzer, D. E. Kharzeev, Heavy quark colorimetry of QCD matter, Phys. Lett. B 519 (2001) 199–206. [arXiv:hep-ph/0106202](#), [doi:10.1016/S0370-2693\(01\)01130-3](#).
90. S. Wicks, W. Horowitz, M. Djordjevic, M. Gyulassy, Elastic, inelastic, and path length fluctuations in jet tomography, Nucl. Phys. A 784 (2007) 426–442. [arXiv:nuc1-th/0512076](#), [doi:10.1016/j.nuclphysa.2006.12.048](#).
91. W. Ke, Y. Xu, S. A. Bass, Linearized Boltzmann-Langevin model for heavy quark transport in hot and dense QCD matter, Phys. Rev. C 98 (6) (2018) 064901. [arXiv:1806.08848](#), [doi:10.1103/PhysRevC.98.064901](#).

92. T. Renk, Biased showers: A common conceptual framework for the interpretation of high- P_T observables in heavy-ion collisions, Phys. Rev. C 88 (5) (2013) 054902. [arXiv:1212.0646](#), [doi:10.1103/PhysRevC.88.054902](#).
93. H. Agakishiev, et al., Studies of di-jet survival and surface emission bias in Au+Au collisions via angular correlations with respect to back-to-back leading hadrons, Phys. Rev. C 83 (2011) 061901. [arXiv:1102.2669](#), [doi:10.1103/PhysRevC.83.061901](#).
94. ATLAS Collaboration, Measurement of jet fragmentation in Pb+Pb and pp collisions at $\sqrt{s_{NN}} = 5.02$ TeV with the ATLAS detector, Phys. Rev. C 98 (2) (2018) 024908. [arXiv:1805.05424](#), [doi:10.1103/PhysRevC.98.024908](#).